Chemosphere 235 (2019) 586–595

Contents lists available at ScienceDirect

Chemosphere

journal homepage: www.elsevier.com/locate/chemosphere

Photochemical release of dissolved organic matter from particulate organic matter: Spectroscopic characteristics and disinfection by-product formation potential

Han-Saem Lee [a], Jin Hur [b], Mi-Hee Lee [b], Simona Retelletti Brogi [b], Tae-Wook Kim [a], Hyun-Sang Shin [a, *]

[a] Department of Environmental Energy Engineering, Seoul National University of Science & Technology, Seoul 01811, South Korea
[b] Department of Environment & Energy, Sejong University, Seoul 05006, South Korea

HIGHLIGHTS

- DOC from both soil and litter leaves were enhanced by UV irradiation.
- The humic-like component mainly generated in soil and protein-like in leaves.
- Photochemically released DOM produced by desorption in soil, dissolution in leaves.
- THM and HAA precursor were mainly produced by light from soil and BL, respectively.
- Specific DBPFP highly correlated with PARAFAC components for soil, $SUVA_{254}$ for leaves.

GRAPHICAL ABSTRACT

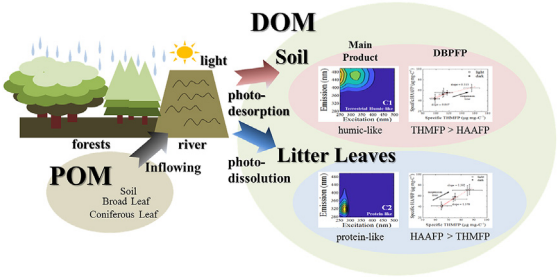

ARTICLE INFO

Article history:
Received 8 March 2019
Received in revised form
31 May 2019
Accepted 17 June 2019
Available online 19 June 2019

Handling Editor: Jun Huang

Keywords:
Photoproduction
Soil
Leaves
EEM-PARAFAC
THMFP
HAAFP

ABSTRACT

In this study, we investigated the photochemical release of dissolved organic matter (DOM) from the particulate organic matter (POM) of soil and litter leaves (broad leaves; coniferous leaves) and compared the releasing characteristics of the DOM using UV-visible and fluorescence spectroscopy. The disinfection by-product formation potential (DBPFP) of the released DOM was also examined. Additional dissolved organic carbon (DOC) was released by UV irradiation for all POM sources (10.58 ± 2.7 mg-C L^{-1} g^{-1} for BL, 8.32 ± 2.6 mg-C L^{-1} g^{-1} for CL, and 0.20 ± 0.1 mg-C L^{-1} g^{-1} for soil). The excitation-emission matrix combined with parallel factor analysis results showed that the photo-released DOM from soil was mainly humic-like components (C1, C3) produced by photodesorption, resulting in high trihalomethane formation potential, while protein-like component (C2) was the major component of the photodissolved DOM from litter leaves, resulting in high haloaceticacid formation potential. Further, DBPFP from soil and litter leaves showed high correlation with humic-like components (C1+C3) and $SUVA_{254}$, respectively. In conclusion, this study demonstrates that significant amounts of DOM could be released from POM under UV irradiation, although the characteristics and DBP formation of the photo-released DOM were highly dependent upon the POM source.

* Corresponding author..
E-mail address: hyuns@seoultech.ac.kr (H.-S. Shin).

https://doi.org/10.1016/j.chemosphere.2019.06.127
0045-6535/

1. Introduction

Particulate organic matter (POM) is typically classified as ranging from 0.45 μm to 2 mm in size fractions of particles with organic matter. Many rivers in regions with a monsoon climate receive considerable POM loading from upstream catchments during a short period in the high flow season (Chen et al., 2006; Hur et al., 2007; Osburn et al., 2012). For example, it was reported that over 80% of the annual particulate organic carbon (POC) flowed into a river during heavy rain events (Lee et al., 2016). Although most relatively large-sized POM is precipitated when it enters into rivers (He et al., 2016b), smaller sized POM, as with silt and clay, might be suspended for a long period of time (Southwell et al., 2010). This suspended POM might further undergo photochemical reactions and release DOM in sunlight, which would supply enormous quantities of DOM and nutrients into riverine systems (Shin et al., 2004; Hur et al., 2007; Mayer et al., 2012; Worrall et al., 2018). Moreover, the photo-released DOM from POM could serve as potential precursors for genotoxic, mutagenic, and carcinogenic disinfection byproducts (DBPs) upon reaction with oxidants in water treatment plants (Pifer and Fairey, 2014; Yang et al., 2015; Golea et al., 2017; Lee et al., 2018). Despite such expected impacts, the potential of POM to be a significant source of DOM has been often overlooked in comparison with other major DOM sources.

Over the past three decades, a number of studies have broadened the scientific knowledge with regard to the interactions between DOM and POM in the water column (Butman et al., 2007; Mayer et al., 2009; Chen and Hur, 2015; He et al., 2016a, 2016b; Liu and Shank, 2015). In particular, the photochemical effects on POM have been primarily conducted using DOM samples extracted from particulate matter through an alkaline solution or water (Osburn et al., 2012; He et al., 2016a). However, as described by Zimmermann-Timm (2002), it is more reasonable to conduct such photochemical investigations of POM using a suspended fraction of particle matter (PM) rather than a bulk one, because the settled PM fraction may have different exchange processes from suspended particles. There are only a few studies of DOM-POM interactions using suspended PM. However, most of them only focused on re-suspended sediments. For example, Koelmans and Prevo (2003) reported that the disturbance of sediments played an important role in dissolved organic carbon (DOC) formation when particulate carbon bound to sediments is mobilized and desorbed. Kieber et al. (2006) and Shank et al. (2011) conducted sediment re-suspension experiments using bottom sediments and overlying water in the presence of light, and observed the measurable dissolution of organic carbon from sediments. Recently, POM from specific sources such as suspended soils has been studied rather than sediments of an uncertain origin (Mayer et al., 2012). Mayer et al. (2012) reported that up to a third of POC in soil appeared in the form of photodissolved organic carbon through continuous exposure to full-strength sunlight for 12 h. However, there are still a number of uncertainties regarding the properties of POM sources, particularly in regard to its photo-releasing mechanism in water such as photodissolution and photodesorption, and its impacts on aquatic environments.

Spectroscopic analyses have been widely applied in characterizing DOM (Li et al., 2014; Yu et al., 2015; Yang et al., 2017b). Ultraviolet-visible (UV-vis) spectroscopy has been employed to identify the composition and reaction of chromophoric dissolved organic matter (CDOM), a pool of light-absorbing DOM. Fluorescence excitation-emission matrix (EEM) combined with parallel factor analysis (PARAFAC) has been used to estimate the relative composition of fluorescent dissolved organic matter (FDOM) depending on the fluorescence feature (Mostofa et al., 2007; Timko et al., 2015; Phong and Hur, 2015; Maqbool and Hur, 2016). In recent studies, EEM-PARAFAC has been primarily applied to investigate the photodegradation of FDOM from suspended PM (Shank et al., 2011; Osburn et al., 2012). Shank et al. (2011) have suggested that the DOM produced during the photodissolution and/or photodesorption of sediments primarily includes humic-like components using EEM-PARAFAC.

In this study, we examined the photochemical release of DOM from suspended POM by UV irradiation. Further, we characterized the photo-released DOM using UV-vis spectroscopy and EEM-PARAFAC analysis and examined their association with the formation of DBPs. The POM sources used in this study included three different organic materials (soil, broad leaves, and coniferous leaves) that are likely to be dominantly distributed in forested watersheds. The primary objectives of this study were (1) to investigate the changes in spectroscopic characteristics of the DOM (e.g., CDOM, FDOM) derived from suspended POM samples using spectroscopic analysis, and (2) to examine the specific DBP formation potential (DBPFP) of the produced DOM to identify the potential relationships between the DBPFP and measured DOM properties.

2. Methods and materials

2.1. Samples collection

In order to compare different POM sources, the samples included soil and two types of leaf litter: deciduous broad leaves (BL) and coniferous leaves (CL). The samples were collected before the rainy season in May 2016, in the Han River basin, South Korea (N 37° 32′ 54.1″ E 127° 19′ 8.6″). The soil was sampled from a depth of 0–5 cm at a location surrounded by vegetation near the river. The litter leaves were also obtained from the forest floor close to the soil sample. The dominant species of the collected leaves were *Quercus mongolica* for BL and *Pinus densiflora* for CL. The collected samples were fully air-dried in a well-ventilated location for 24 h and the litter leaves were ground into small pieces (<200 μm) using a grinder (Mayer et al., 2012; Lee and Hur, 2014) prior to use. The carbon contents of the particle samples were analyzed using an elemental analyzer (Vario macro cube, Elementar, Germany), and were 1.8% for soil and 49.2% and 49.4% for BL and CL, respectively (Table S1).

2.2. Suspension solution preparation and UV irradiation experiments

The suspension solutions for UV irradiation were prepared by immersing the POM samples in deionized water at concentrations of 20,000 mg L^{-1} for soil, 500 mg L^{-1} for BL, and 500 mg L^{-1} for CL (Mayer et al., 2012). The sample concentrations were determined based on the consideration of the typical DOC concentration range (5-15 mg-C L^{-1}) in the Han River (the largest river in South Korea) during rainfall season (Water Information System, 2018). The organic carbon values for each sample were 360 mg-C L^{-1} for soil, 246 mg-C L^{-1} for BL, and 248 mg-C L^{-1} for CL based on the total organic carbon (TOC) concentrations measured by the elemental analyzer. After 30 min of shaking at 300 rpm for sample homogenization, each solution was divided into two equal parts. One part underwent UV irradiation, whereas the other part was kept in the dark as a control. The initial DOC concentrations of the suspension solutions were 8.46 mg-C L^{-1} for soil, 8.60 mg-C L^{-1} for BL, and 10.33 mg-C L^{-1} for CL, and the initial pH of the suspension solutions ranged from 5.0 to 6.0.

In order to investigate the more obvious impact of photo-releasing effect of DOM from different POM sources, UVA, which accounts for 95% of UV reaching the ground surface and has a large

influence on DOM production from POM, was used as the light source of this experiment (Kieber et al., 2006; Zhang et al., 2009; Hu et al., 2016). UV irradiation was conducted in a closed cabinet equipped with twelve 8W-UVA lamps (F8T5BL, Sankyo Denki, Japan) as a light source, and the lamp wavelength was set at 352 nm (Phong and Hur, 2015). Each suspension group was stirred at 300 rpm in a cylindrical quartz reactor and then placed in the middle of the cabinet to ensure equal exposure to the UV light. The temperature in the cabinet was maintained at 25 ± 3 °C by circulating cooling air with a fan. A UVA intensity of 1.5 ± 0.2 mW cm^{-2}, equivalent to the average sunlight intensity at noon during summer in the middle regions (137° 29′ N) of Korea (Hur et al., 2011; Lee and Hur, 2014), was used for irradiation. The 30 mL aliquots were taken from 1 L of suspension solution at 1, 6, 12, 24, and 48 h, respectively. These samples were immediately filtered using a pre-washed 0.45 μm membrane filter to remove the remaining particles, and stored at 4 °C in the dark. All of the experiments were conducted in duplicate.

2.3. DOC concentration, and UV-visible and fluorescence spectra

The DOC concentration (mg-C L^{-1}) was measured with a TOC analyzer (Vario TOC select, Elmentar, Germany). The absorption spectra were obtained by scanning absorbance at the wavelengths from 200 nm to 500 nm with 1-nm resolution using a UV-visible spectrophotometer (UV-1800, Shimadzu, Japan). Fluorescence EEMs were measured with a spectrofluorometer (Hitachi, F-7000, Japan). All samples were optically diluted (UV_{254} $cm^{-1} < 0.05$) before measuring the EEMs (Murphy et al., 2008; Hur et al., 2009). The measured excitation and emission wavelengths were set from 250 to 500 nm and from 280 to 550 nm with scan steps of 5 nm and 1 nm, respectively. The EEM of deionized water was used as a blank and subtracted from all of the EEMs. The EEMs were normalized using Raman integrated area (Murphy et al., 2013; Maqbool and Hur, 2016).

Absorption coefficients (a) were calculated by multiplying UV absorbance at 254 nm by 2.303 and then dividing by pathlength (Helms et al., 2008). Specific UV absorbance (SUVA) values were determined by dividing the UV absorbance at 254 nm with the DOC concentrations (Weishaar et al., 2003). The spectral slope ratio (S_R) was determined by calculating the ratio of the slope of the shorter wavelength region (275–295 nm) to that of the longer wavelength region (350–400 nm) (Helms et al., 2008). The humification index (HIX) was calculated as the ratio of the area under the emission spectra over 435–480 nm to that over 300–345 nm, obtained at excitation 254 nm (Zsolnay et al., 1999). The fluorescence index (FI) refers to a ratio of the emission intensities at 450–500 nm with a fixed Ex of 370 nm (McKnight et al., 2001). The biological index (BIX) was estimated using a ratio of the emission intensities at 380–430 nm at excitation 310 nm (Huguet et al., 2009). PARAFAC modeling was performed on EEMs of samples from all three origins by using drEEM toolbox (Murphy et al., 2013) in MATLAB R2017a (Mathworks, Natick, MA, USA). The EEM data for the PARAFAC modeling were obtained based on 36 EEM data from 6 separate experiments. Detailed information about the PARAFAC analysis of the EEM spectra can be found elsewhere (Murphy et al., 2013). Statistical analysis was conducted by using SPSS statistics program (Version 18.0).

2.4. Specific DBPFP test

The solutions for the specific DBPFP test were all diluted to a constant concentration of 1 mg-C L^{-1} prior to chlorination. Chlorination was achieved by adding sodium hypochlorite to the solutions at a sufficient chlorine dosage (NaOCl, Aldrich, >4% available chlorine) of 5 mg-Cl_2 mg-C^{-1}. The chlorinated solutions were quickly sealed headspace-free and incubated in the dark at 25 °C for 24 h. The specific DBPFP was operationally defined as four trihalomethane (THM, chloroform, bromodichloromethane, dibromochloromethane, bromoform) and three haloacetic acid (HAA, dichloroacetic acid, trichloroacetic acid, dibromoacetic acid) species formed upon chlorination (Pifer and Fairey, 2012, 2014; Lee et al., 2018). The THMs were pretreated using purge and trap (purging 11 min, desorption at 200 °C for 2 min) and analyzed using gas chromatography-mass spectrometry (GC-MS, 7890B-5977A, Agilent, USA). Additionally, the HAAs were analyzed using gas chromatography-electron capture detector (GC-ECD, CP-3800, Bruker, Germany). The detailed operating conditions are described in Table S2.

3. Results and discussion

3.1. Changes in released DOC during UV irradiation

Photo-exposure of the suspended POM from the soil and leaves resulted in a high amount of DOC production (Fig. 1). Normalized to the particle weight (g-dry), the DOC concentrations (mg-C L^{-1} g^{-1}) under UV irradiation from the POM continuously increased and reached a maximum value of 1.00 ± 0.09 mg-C L^{-1} g^{-1} (from 0.42 ± 0.01 mg-C L^{-1} g^{-1}) for soil, 39.31 ± 2.60 mg-C L^{-1} g^{-1} (from 17.21 ± 0.47 mg-C L^{-1} g^{-1}) for BL, and 32.99 ± 2.27 mg-C L^{-1} g^{-1} (from 20.66 ± 0.49 mg-C L^{-1} g^{-1}) for CL over a period of 48 h. In contrast, relatively lower values were observed in the dark control over the time: 0.80 ± 0.06 mg-C L^{-1} g^{-1} for soil, 28.73 ± 0.88 mg-C L^{-1} g^{-1} for BL, and 24.67 ± 1.29 mg-C L^{-1} g^{-1} for CL. Similarly, Kieber et al. (2006) and Shank et al. (2011) found that the DOC concentrations from various sediments were elevated with simulated sunlight, and they reported that organic matter loosely bound to sediment particulate surfaces could be further released. On the other hand, the DOC of each origin accounted for 5.55%, 7.99%, and 13.30% of initial TOC in soil, BL and CL, respectively, at 48 h UV irradiation.

For a proper comparison with previous studies, the so-called DOC photoproduction (mg-C L^{-1} g^{-1} h^{-1}) was calculated by subtracting the DOC of the control sample from the values of the UV-irradiated samples at 48 h and dividing it by the total suspension time (h). The DOC photoproduction per hour for samples was 0.004 ± 0.001 mg-C L^{-1} g^{-1} h^{-1} for soil, 0.220 ± 0.036 mg-C L^{-1} g^{-1} h^{-1} for BL, and 0.173 ± 0.020 mg-C L^{-1} g^{-1} h^{-1} for CL. The higher rate of DOC photoproduction in litter leaves versus soil can be attributed to the more enriched carbon content in litter leaves (49.2–49.4%) than in soil (1.8%) (Table S1). A previous study by Kieber et al. (2006) showed that the DOC photoproduction from sediments ranged from 0.004 mg-C L^{-1} g^{-1} h^{-1} to 0.200 mg-C L^{-1} g^{-1} h^{-1} through a 9 h of irradiation, which was comparable to the results of this study. Hu et al. (2016) observed a DOC photoproduction of 0.037 mg-C L^{-1} g^{-1} h^{-1} to 0.157 mg-C L^{-1} g^{-1} h^{-1} from the Taihu Lake sediment through 8 h of irradiation. These results might suggest that the DOC photoproduction rate was relatively lower in soil than in sediments. On the other hand, the DOC_{light}/DOC_{dark} ratio of soil was slightly higher (1.49) than that of leaves (1.29–1.37) at 48 h (Fig. S1), suggesting that the POM of soil was more actively converted into DOM upon UV irradiation compared to those of leaves. Therefore, the results indicate that the DOC photoproduction by UV irradiation could be greatly influenced by the POM source as well as the POM content.

3.2. Changes in spectroscopic characteristics of DOM during UV irradiation

Various optical indices obtained for the photo-released DOM are

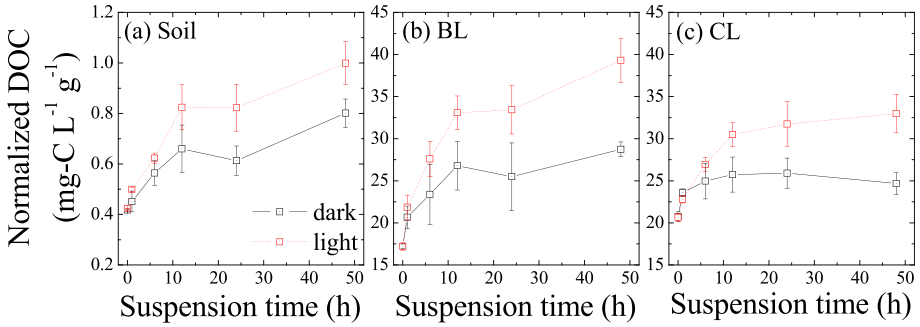

Fig. 1. Changes in normalized dissolved organic carbon (DOC, mg-C L^{-1} g^{-1}) of (a) soil, (b) broad leaves (BL), and (c) coniferous leaves (CL) in the presence and absence of UV irradiation with respect to suspension time.

presented in Table 1. During the suspension, the absorption coefficient ($a_{254,}$ m^{-1}), which reflects the abundance of CDOM fractions (Chen and Jaffé, 2014), showed increases in both light and dark conditions irrespective of the POM sources. The increase of the CDOM from POM was higher in the light versus the dark condition. In comparison with the initial value, over a period of 48 h, the a_{254} in soil increased by 1.8 times in the dark, while it increases by 2.6 times under UV irradiation. Likewise, the a_{254} in BL and CL increased by 2.1 and 1.4 times, respectively, in the dark, and while it rose by 2.9 and 2.2 times in the light. The increase of CDOM in both dark and light conditions could be explained by desorption and/or dissolution of CDOM components from POM (Shank et al., 2011). On the other hand, although the soil with higher POM concentration than leaves showed lower DOC production than leaves after 48 h of UV irradiation, the a_{254} of DOM from the soil was higher (149.7 m^{-1}) than those from litter leaves (BL 122.1 m^{-1}; CL 71.4 m^{-1}). These results agree with those from Garcia et al. (2018), who observed that DOM derived from soil had higher aromaticity and lignin content compared with the DOM from litter leaves.

SUVA, which is an indicator of DOM aromaticity (Weishaar, 2003), increased for all of the origins during the suspension. However, no distinct differences were observed between light and dark conditions. The SUVA at 48 h was 2.95 L mg-C^{-1} m^{-1} for soil, 2.93 L mg-C^{-1} m^{-1} for BL, and 0.81 L mg-C^{-1} m^{-1} for CL in dark conditions, while the values under UV irradiation were 2.84 L mg-C^{-1} m^{-1}, 2.80 L mg-C^{-1} m^{-1}, and 0.99 L mg-C^{-1} cm^{-1}, respectively. These results indicate that the aromaticity of the POM-released DOM is not affected by UV irradiation, despite the increasing trend of CDOM from the suspended POM. The results suggest that when the POM is irradiated with UV light, non-CDOM fraction (i.e., non-UV-absorbing compounds) could be equally released from the POM. Another plausible explanation is that the existing CDOM could lose its optical properties by photodegradation and/or photobleaching (Hur et al., 2011; Chen and Jaffé, 2014; Garcia et al., 2018). The SUVA value was the lowest for the CL (<1 L mg-C^{-1} m^{-1}) and higher for both soil and BL, ranging from 1.84 to 2.95 L mg-C^{-1} m^{-1} during the UV irradiation.

The spectral slope ratio (S_R) was proposed as an indicator for tracking the changes in the ratios of low-molecular-weight to high-molecular-weight (LMW/HMW) DOM (He et al., 2016a). In this

Table 1
Changes in pH and spectroscopic indexes for different origins of particulate organic matter (POM) with respect to suspension time.

Origin	time (h)	pH		a_{254}[a] (m^{-1})		$SUVA_{254}$[b] (Lmg-$C^{-1}m^{-1}$)		S_R[c]		HIX[d]		FI[e]		BIX[f]	
		dark	light	dark	light	dark	light	dark	light	dark	light	Dark	light	dark	light
Soil	0	6.0	6.0	57.6	57.6	2.07	2.07	4.08	4.18	2.28	2.42	1.41	1.59	0.50	0.49
	1	5.9	5.9	64.5	71.4	2.22	2.20	4.28	4.20	3.14	3.27	1.41	1.40	0.50	0.51
	6	6.0	6.1	78.3	94.4	2.31	2.30	4.18	4.13	2.55	2.78	1.46	1.40	0.49	0.49
	12	6.1	5.9	92.1	112.9	2.37	2.31	3.63	3.95	2.89	3.81	1.43	1.41	0.50	0.50
	24	5.9	5.9	119.8	126.7	2.81	2.74	2.95	3.13	2.11	3.50	1.50	1.39	0.51	0.56
	48	5.9	6.0	105.9	149.7	2.95	2.84	2.83	3.09	4.19	5.83	1.42	1.41	0.61	0.57
BL	0	5.7	5.7	43.8	41.5	1.84	1.84	3.37	3.32	1.67	1.65	1.59	1.60	0.78	0.89
	1	5.7	5.7	48.4	50.7	1.96	1.94	3.35	3.55	1.26	1.17	1.58	1.52	0.85	1.04
	6	5.6	5.5	62.2	71.4	2.15	2.23	3.48	3.72	1.79	1.20	1.57	1.49	0.86	1.04
	12	5.6	5.5	71.4	87.5	2.26	2.39	3.48	3.72	1.27	1.15	1.55	1.44	1.06	1.95
	24	5.5	5.5	76.0	99.0	2.66	2.61	3.31	3.54	1.64	1.01	1.61	1.41	1.12	0.87
	48	6.3	5.9	89.8	122.1	2.93	2.80	3.21	3.56	1.48	1.36	1.32	1.56	0.82	1.32
CL	0	5.7	5.6	32.2	32.2	0.69	0.70	6.86	6.80	0.56	0.61	2.06	1.95	0.85	0.82
	1	5.6	5.5	36.9	36.9	0.69	0.74	6.40	7.45	0.63	0.69	1.95	1.98	0.85	0.85
	6	5.6	5.4	41.5	48.4	0.76	0.82	5.08	6.66	0.71	0.46	2.03	1.82	0.86	0.84
	12	5.6	5.4	43.8	53.0	0.80	0.82	5.05	6.50	0.69	0.48	2.03	1.67	0.89	0.77
	24	5.7	5.3	43.8	57.6	0.83	0.96	5.77	6.11	0.73	0.42	2.06	1.53	0.90	0.77
	48	6.4	5.1	46.1	71.4	0.81	0.99	6.16	6.33	0.69	0.41	1.86	1.36	0.90	0.68

[a] Napierian absorption coefficient (a) calculated by multiplying UV absorbance at 254 nm by 2.303 and then dividing by path length (Helms et al., 2008).
[b] Specific UV absorbance (SUVA) values were determined by dividing the UV absorbance at 254 nm with the DOC concentrations (Weishaar et al., 2003).
[c] Spectral slope ratio (S_R) was determined by calculating the ratio of the slope of the shorter wavelength region (275–295 nm) to that of the longer wavelength region (350–400 nm) (Helms et al., 2008).
[d] Humification index (HIX) was calculated as the ratio of the area under the emission spectra over 435–480 nm to that over 300–345 nm, obtained at excitation 254 nm (Zsolnay et al., 1999).
[e] Fluorescence index (FI) refers to a ratio of the emission intensities at 450–500 nm with a fixed Ex of 370 nm (McKnight et al., 2001).
[f] Biological index (BIX) was estimated using a ratio of the emission intensities at 380–430 nm at excitation 310 nm (Huguet et al., 2009).

study, the S_R values showed a difference depending on the POM origins. The initial S_R value of the DOM from BL was as low as 3.3, compared with those of the soil (4.2) and CL (6.8). Notably, the S_R values of DOM from BL and CL did not show significant changes and resulted in 3.5 and 6.3 after 48 h of UV irradiation, respectively. In contrast, the value in the soil decreased by about 26%, from 4.2 to 3.1. The results suggest that both the LMW and HMW fractions in the litter leaves were released during the UV irradiation, while, in the soil, the HMW fraction might be preferentially released by the light. This interpretation is supported by Garcia et al. (2018), who reported that the DOM derived from leaves could consist of both small biodegradable molecules and large non-humic compounds such as carbohydrates and proteins, while the HMW from the soil might be mostly humic substances with macromolecules.

Similar to the above results, the HIX, or humification index (Zsolnay et al., 1999), showed an increase only for the soil and no distinct change for litter leaves after UV irradiation. Over 48 h, the HIX of the soil increased from 2.42 to 5.83, suggesting that the DOM molecules, with higher degrees of the condensation in aromatic structures and the conjugation in unsaturated aliphatic chains, are likely to be preferentially released from the soil POM (He et al., 2016a). A lower FI and BIX indicate more aged terrestrial-derived DOM, while a higher FI and BIX indicate fresher microbial-derived DOM. The initial FI and BIX for soil were the lowest values (1.59, 0.49, respectively) of all origins; those of CL exhibited higher values (1.95, 0.82) in comparison to those of soil. While the FI of BL was similar to that of soil (1.60) and BIX of BL was initially consistent with that of CL (0.89). The results confirmed that the DOM from soil has a higher degree of humification in carbon structures and less biological/microbial contribution in comparison with DOM from CL (Lee et al., 2018). The DOM from BL seemed to be similar to that of the soil with regard to the composition, although the production pathway might be similar to that of the CL.

3.3. Changes in PARAFAC components during UV irradiation

In order to more accurately examine the photochemical effect, the EEMs of the photo-released DOM from the suspended POM were measured and their signals were decomposed to three main fluorescent components (C1, C2, and C3) by PARAFAC modeling (Fig. 2). The three fluorescent components were assigned based on the similarity >92% obtained by using the OpenFluor database (Table S3) (Murphy et al., 2014). For C1, fluorescence maxima were at Ex/Em of <250(330)/470 nm. This component was a combination of widespread peak A and C and defined as a terrestrial humic-like component (Catalá et al., 2015; Dainard et al., 2015; Nimptsch et al., 2015; Soto Cárdenas et al., 2017; Derrien et al., 2018). Lee et al. (2015) stated that the C1 components with longer emission wavelengths likely corresponded to the larger molecular size of a terrestrial humic-like component. The C2 displayed fluorescence maxima at Ex/Em of 275/320 nm, indicating the presence of a tryptophan-like component (peak T) which is typically a protein-like component. The C3 had fluorescence maxima at Ex/Em of 300(<250)/358 nm. This component typically exhibited a combination of peak A and M and was assigned to a microbial humic-like substance (Yamashita and Jaffé, 2008; Graeber et al., 2012; Murphy et al., 2013; Chen and Jaffé, 2014). The C3 has been considered as an intermediated product with DOM that had a relatively low molecular size compared to that of C1 Hur (2011), Chen and Jaffé (2014).

The relative distribution of the three fluorescent components (C1, C2, and C3) for the DOM from the POM of the soil and litter leaves displayed some initial differences (Fig. S2). The DOM from the soil POM presented the highest abundance of C1 (58.2%), followed by C2 (23.9%) and C3 (17.9%). Such a high presence of C1 was also found in the DOM derived from agricultural soil (Yamashita and Jaffé, 2008). The DOM from BL was found to be 45.5% for C1, 24.5% for C2, and 30.0% for C3, respectively. Unlike in the BL and soil, CL had the highest relative distribution of C2 (61.1%) with the lowest presence of C1 (22.3%) and C3 (16.6%), suggesting that there is a high abundance of the protein-like component in CL. Similarly, Cuss and Guéguen (2013) reported that the protein-like fluorescence was highly dominant in the leachates of spruce needles and that they might be associated with quinones, lignins, polyphenols, and tannin-like structures.

The fluorescence maximum intensity (F_{max}) for soil was in the range of 0.3–11.0, while that for litter leaves ranged from 0.3 to 1.9, indicating that the FDOM components produced by UV irradiation were higher for the soil than for leaves (Fig. S2). Fig. 3 shows the change in the ΔF_{max} (i.e., $F_{max\text{-}light}$-$F_{max\text{-}dark}$) of fluorescence components in the photo-released DOM molecules from each source of POM samples. The soil-derived FDOM did not show any distinct change during the 24 h period, however, the humic-like components (i.e., C1 and C3) increased by ~3 times in comparison with the dark condition after 48 h. On the other hand, in the regard to the litter leaves, the protein-like component (C2) increased by ~1.5 times in both BL and CL within 6 h, and the humic-like components of litter leaves were consistent or slightly reduced by UV irradiation during the 48 h period. These results confirm that the increase in the FDOM fraction of soil and litter leaves was mainly due to the release of the humic-like and the protein-like components, respectively.

Furthermore, with regard to the changes in the S_R value and PARAFAC components, the main exchange mechanism between POM and DOM could differ between soil and litter leaves. In mineral-based soils, it could be inferred that the DOM with more aromatic, carboxyl, and hydrophobic fractions (i.e., humic-like substances) was generated by the exposure to UV light after a relatively long suspension time (>24 h). Because it has previously been observed that high hydrophobic fractions were preferentially adsorbed on the mineral surface by hydrophobic interactions (Hur and Schlautman, 2003; Kleber et al., 2007; He et al., 2016b); thus, the DOM photo-released from the soil POM might occur through photodesorption in the reverse direction of the adsorption mechanism suggested by Kleber et al. (2007). In contrast, the DOM derived from litter leaves was produced in constant molecular weight and large non-humic compounds (i.e., protein-like substances) for a relatively short suspension time (<6 h). These results could indicate that the POM of litter leaves (i.e., macroaggregates) was primarily solubilized into DOM (e.g., polysaccharides and proteins) through the pathways of fragmentation, dispersion, and dissociation (i.e., photodissolution) (Goldthwait et al., 2005; He et al., 2016b).

3.4. Specific DBPFP of DOM and relationship with spectroscopic indicators

The specific DBPFP of the photo-released DOM increased in soil and BL during the suspension of POM, although not in CL (Fig. S3). Initial values of the specific DBPFP were the highest for soil, 142.98 ± 5.64 μg/mg-C, followed by 106.70 ± 7.18 μg/mg-C for BL and 61.96 ± 13.96 μg/mg-C for CL. Over the 48 h period, the specific DBPFP in the dark increased by about 10–20 μg/mg-C in the suspension of all POM, while it further increased under UV irradiation only for soil and BL. DBP precursors have been known to be removed by photodegradation (Lee and Hur, 2014; Ruecker et al., 2017). However, our results showed that the DBPFP of DOM was enhanced even in the presence of UV irradiation, which can be explained mainly by the further increase of photo-released CDOM and FDOM from the POM of soil and BL under UV irradiation, which

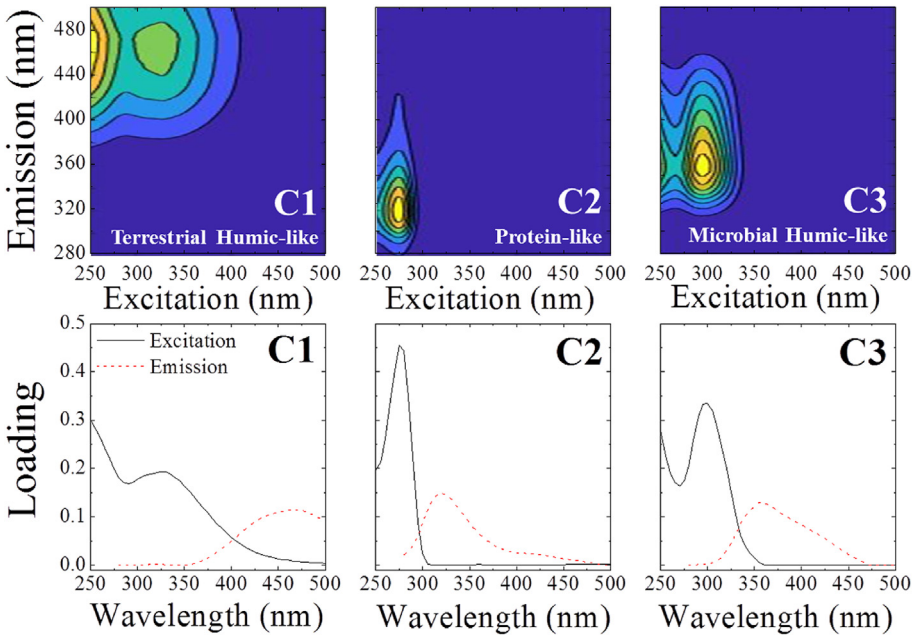

Fig. 2. Identified PARAFAC components (C1-C3) and their excitation and emission spectra.

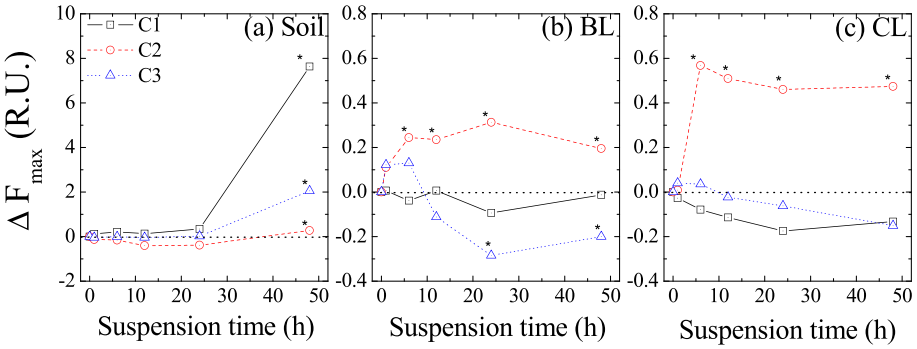

Fig. 3. Changes in Δ fluorescent maximum intensity (i.e., $F_{max\text{-}light}$-$F_{max\text{-}dark}$) of each component (C1-C3) in (a) soil, (b) broad leaves (BL), and (c) coniferous leaves (CL) of particulate organic matter (POM) with respect to suspension time, *statistically significant differences between ≤ 24 h and >24 h for soil and ≤6 h and >6 h for leaves (*t*-test by using SPSS, $p < 0.05$).

exceeded the reduced DOM amounts by photodegradation as shown in Table 2 and Fig. 3. On the other hand, the specific DBPFP of the DOM from CL decreased by about 64% under UV irradiation despite the increases in both CDOM and FDOM, suggesting that photo-released DOM from CL may have different DBP precursors in the reaction from the DOM of soil and BL origins. These results may be associated with the previous observation that DOM in CL had a relatively low SUVA value and small humic-like content in comparison with the soil- and the BL-derived DOM, which includes high humic-like DOM structures with higher specific DBPFP.

Regarding DBP species, the slopes of the HAAFP to the THMFP for all POM origins varied under UV irradiation (Fig. 4). In the dark, the slope of HAAFP to the THMFP was 0.647 ± 0.139 for soil, 1.578 ± 0.169 for BL, and 1.798 ± 0.198 for CL, suggesting that the simply leached (i.e., not photo-released) DOM from soil had a higher tendency to form THMs than HAAs, while the litter leaves (BL, CL) showed the opposite trend in regard to specific DBPFP. Under UV irradiation, the slope of HAAFP to THMFP for soil was reduced to 0.313 ± 0.052, suggesting that photo-released DOM from soil has a greater propensity to produce THMs than HAAs. The slope of BL showed no distinct difference between the dark and light conditions, although the amount of both THMFP and HAAFP increased simultaneously by UV irradiation with a similar slope. Notably, for CL, both THMFP and HAAFP decreased by UV irradiation with a slope of 0.406 ± 0.030, which was also in contrast to the results under the dark condition. These results indicate that the photo-released DOM from soil contained more THM precursors than the HAA counterparts and that the DOM from BL included relatively more HAA precursors, while both THM and HAA precursors from the photo-released DOM in CL decreased. The results may suggest that the relatively high increase in THMFP of photo-released DOM from soil resulted from a large increase in humic-like components (i.e., C1, C3), while that in HAAFP of photo-released DOM from BL was mainly attributed to protein-like substances. On the other hand, despite the increase in a_{254} from CL, the decrease in specific DBPFP for CL can be explained by the molecular transformation of the DOM via photodecomposition. Unlike with soil and BL, the fluorescent indexes (i.e., HIX) in CL decreased compared with dark conditions during UV irradiation, indicating that DOM was converted into relatively low humified substances (Derrien et al., 2017; Yang et al., 2017a). As an example to support this, Chen and Jaffé (2014) reported that low molecular weight

Table 2
Correlation between the characteristic indexes of dissolved organic matter (DOM) and the specific disinfection byproduct formation potential (DBPFP) ($n = 18$).

	a_{254} (m^{-1})	SUVA ($m^{-1}L\ mg\text{-}C^{-1}$)	S_R	HIX	FI	BIX	PARAFAC components (R.U.)			C1+C3 (R.U.)	C1+C2+C3 (R.U.)	C1/C2	C1/C3	C2/C3	Specific DBPFP ($\mu g\ mg\text{-}C^{-1}$)		
							C1	C2	C3						THMFP	HAAFP	DBPFP[a]
DOC	0.408	0.119[c]	−0.058[c]	−0.167[c]	−0.222[c]	−0.541[b]	−0.056[c]	−0.265[c]	−0.202[c]	−0.087[c]	−0.122[c]	−0.029[c]	−0.409[c]	−0.179[c]	−0.100[c]	−0.217[c]	−0.064[c]
a_{254}	–	0.803[c]	−0.664[c]	−0.630[c]	−0.658[c]	−0.154[b]	−0.536[c]	−0.268[c]	−0.576[c]	−0.547[c]	−0.504[c]	−0.674[c]	−0.486[c]	−0.509[c]	−0.714[c]	−0.715[c]	−0.805[c]
SUVA	–	–	−0.943[c]	−0.670[c]	−0.713[c]	−0.100[b]	−0.449[c]	−0.678[c]	−0.517[c]	−0.465[c]	−0.367[c]	−0.629[c]	−0.466[c]	−0.844[c]	−0.796[c]	−0.919[c]	−0.919[c]
S_R	–	–	–	−0.665[c]	−0.669[c]	−0.130[b]	−0.404[c]	−0.779[c]	−0.454[c]	−0.416[c]	−0.305[c]	−0.612[c]	−0.458[c]	−0.895[c]	−0.759[c]	−0.873[c]	−0.865[c]
HIX	–	–	–	–	−0.474[c]	−0.488[b]	−0.879[c]	−0.308[c]	−0.831[c]	−0.873[c]	−0.821[c]	−0.961[c]	−0.809[c]	−0.640[c]	−0.910[c]	−0.575[c]	−0.843[c]
FI	–	–	–	–	–	−0.349[b]	−0.328[c]	−0.288[c]	−0.318[c]	−0.328[c]	−0.284[c]	−0.454[c]	−0.440[c]	−0.356[c]	−0.494[c]	−0.527[c]	−0.645[c]
BIX	–	–	–	–	–	–	−0.389[c]	−0.125[c]	−0.165[c]	−0.344[c]	−0.357[c]	−0.414[c]	−0.844[c]	−0.008[c]	−0.417[c]	−0.100[c]	−0.282[c]
C1	–	–	–	–	–	–	–	−0.027[c]	−0.969[c]	−0.999[c]	−0.991[c]	−0.927[c]	−0.636[c]	−0.388[c]	−0.777[c]	−0.411[c]	−0.692[c]
C2	–	–	–	–	–	–	–	–	−0.044[c]	−0.013[c]	−0.152[c]	−0.260[c]	−0.173[c]	−0.883[c]	−0.438[c]	−0.713[c]	−0.540[c]
C3	–	–	–	–	–	–	–	–	–	−0.981[c]	−0.964[c]	−0.895[c]	−0.479[c]	−0.457[c]	−0.755[c]	−0.512[c]	−0.712[c]
C1+C3	–	–	–	–	–	–	–	–	–	–	−0.991[c]	−0.925[c]	−0.606[c]	−0.404[c]	−0.776[c]	−0.434[c]	−0.699[c]
C1+C2+C3	–	–	–	–	–	–	–	–	–	–	–	−0.879[c]	−0.576[c]	−0.279[c]	−0.708[c]	−0.331[c]	−0.618[c]
C1/C2	–	–	–	–	–	–	–	–	–	–	–	–	−0.735[c]	−0.596[c]	−0.875[c]	−0.564[c]	−0.819[c]
C1/C3	–	–	–	–	–	–	–	–	–	–	–	–	–	−0.398[c]	−0.787[c]	−0.320[c]	−0.671[c]
C2/C3	–	–	–	–	–	–	–	–	–	–	–	–	–	–	−0.760[c]	−0.891[c]	−0.804[c]

[a] The sum of THMFP and HAAFP.
[b] $p < 0.05$.
[c] $p < 0.01$.

aromatics, such as polyphenols from the photodecomposition of tannins leached from the biomass materials, could enhance the CDOM signal (i.e., a_{254}). Another plausible explanation is that the decrease in pH of the solution by photo-released DOM from CL may decrease the DBPFP (Lee and Lee, 2015).

Significant correlations between DOM spectral indices and specific DBPFP was found for a_{254}, SUVA, S_R, and HIX, while the FI and BIX showed a low correlation with specific DBPFP (Table 2). The correlation coefficients were 0.805 ($p < 0.01$) for a_{254}, 0.919 ($p < 0.01$) for SUVA, −0.865 ($p < 0.01$) for S_R, and 0.843 ($p < 0.01$) for HIX, respectively, confirming that DOM with higher hydrophobicity, aromaticity, and molecular size have a greater affinity for DBP production (Fig. S4) (Chow et al., 2005, 2006; Hua and Reckhow, 2007; Ruecker et al., 2017). Notably, the SUVA and HIX showed good correlation with specific HAAFP ($r = 0.919$, $p < 0.01$) and THMFP ($r = 0.910$, $p < 0.01$), respectively (Hur et al., 2011; Lee and Hur, 2014). The relationship of PARAFAC components with specific DBPFP showed good positive correlation at both C1 and C3 with THMFP ($r = 0.777$, $p < 0.01$; $r = 0.755$, $p < 0.01$, respectively) and negative correlation for C2 with HAAFP ($r = -0.713$, $p < 0.01$). The results indicated that the major contributor to THM generation could be the humic-like component of the photo-released DOM. Similarly, Pifer and Fairey (2012) reported that the humic-like components of DOM had a high correlation with chloroform production($r^2 = 0.84$). On the other hand, to confirm more detailed differences for the different origins in regards to specific DBPFP, the correlation of specific DBPFP with CDOM (i.e., $SUVA_{254}$) and FDOM (i.e., the sum of fluorescence intensity of humic-like components, C1+C3) was carried out for the soil and litter leaves (both BL and CL) regardless of UV irradiation (Fig. 5). The specific DBPFP of the soil showed a low correlation with a CDOM of 0.699 ($p = 0.122$), but it was high at 0.964 ($p < 0.002$) with the FDOM. On the contrary, that of litter leaves displayed a higher correlation of 0.965 ($p < 0.002$) with CDOM compared with that of FDOM at 0.888 ($p < 0.001$). It seemed that the specific DBPFP of DOM from soil was more closely related to the FDOM fraction, while that from litter leaves was more likely to be involved in CDOM fraction. The differences in the DOM characteristics according to the POM origin has important implications for predicting and managing DBP generation in terms of raw water management (Hua and Reckhow, 2007; Chow et al., 2008; Lee and Hur, 2014). In this study, the fluorescent PARAFAC components (i.e., C1+C3) and $SUVA_{254}$, which best reflect different characteristics of the DBP precursor by POM sources, seemed appropriate indexes for the DBP production of DOM from soil and litter leaves, respectively.

4. Conclusions

In this study, the photo-released DOC content (mg-C L^{-1} g^{-1}) was about 30 times higher for leaves than for soil (33–39 *versus* 1.0), but the DOC_{light}/DOC_{dark} ratio increased more in soil under UV irradiation, which indicates that the POM of soil was more actively converted to DOM upon UV irradiation compared to leaves. The spectral indices (a_{254}, SUVA, S_R, HIX, FI, and BIX) and PARAFAC components revealed that the photo-released DOM from soil was mainly composed of humidified humic-like molecules with high degrees of aromatic character and molecular weight, which was driven by photodesorption, while in the litter leaves, photodissolution of protein-like components with similar molecular weight seemed to be the governing releasing process. Both THMFP and HAAFP of the photo-released DOM were further increased by UV irradiation for soil and BL. The DBPFP of the DOM of soil and litter leaves showed good correlation with humic-like components (i.e., C1+C3, $r = 0.964$, $p < 0.002$) and $SUVA_{254}$ ($r = 0.965$, $p < 0.002$), respectively. The findings of this study provided

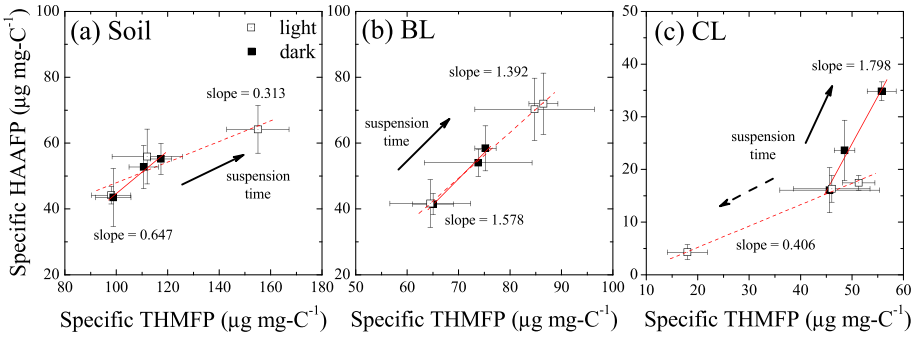

Fig. 4. Changes in the slopes of specific haloacetic acid formation potential (HAAFP) to the specific trihalomethane formation potential (THMFP) for different origins (a) soil, (b) broad leaves (BL), and (c) coniferous leaves (CL) in the presence and absence of UV irradiation (arrow direction indicates the elapsed suspension time from initial to 48 h; the solid and dash type of arrow in (c) represents the dark and light conditions).

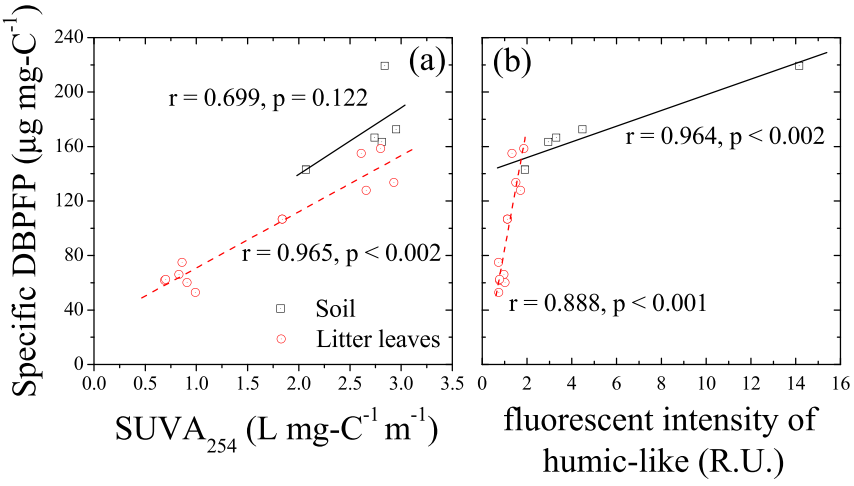

Fig. 5. Correlation of specific disinfection byproduct formation potential (DBPFP) with (a) specific UV absorbance at 254 nm ($SUVA_{254}$; i.e., CDOM) and (b) the sum of fluorescence intensity of humic-like components (i.e., C1+C3; FDOM) depending on the particulate organic matter (POM) sources ($n = 6$).

scientific knowledge on the characteristics of photo-released DOM (content, molecular composition, and releasing mechanism, DBPFP, etc.) from soil and litter leaves, the dominantly distributed POM sources in the forest watershed, which can help to broaden our understanding of the environmental impacts of particulates entering into the water body during rainfall.

Acknowledgments

This work was supported by a National Research Foundation of Korea grant funded by the Korea government (MSIP) (No.2017R1A2A2A09069617).

Appendix A. Supplementary data

Supplementary data to this article can be found online at https://doi.org/10.1016/j.chemosphere.2019.06.127.

Contribution

Han-Saem Lee, Jin Hur, and Hyun-Sang Shin designed the research plan.

Han-Saem Lee conducted experiments and wrote the manuscript with support from Jin Hur, Mi-Hee Lee, Simona Retelletti Brogi, and Hyun-Sang Shin.

Han-Saem Lee conducted PARAFAC analysis with support from Simona Retelletti Brogi.

Tae-Wook Kim analyzed the disinfection by-products.

References

Butman, D., Raymond, P., Oh, N.-H., Mull, K., 2007. Quantity, ^{14}C age and lability of desorbed soil organic carbon in fresh water and seawater. Org. Geochem. 38 (9), 1547–1557.

Catalá, T.S., Reche, I., Fuentes-Lema, A., Romera-Castillo, C., Nieto-Cid, M., Ortega-Retuerta, E., Calvo, E., Álvarez, M., Marrasé, C., Stedmon, C.A., Álvarez-Salgado, X.A., 2015. Turnover time of fluorescent dissolved organic matter in the dark global ocean. Nat. Commun. 6, 5986.

Chen, M., Hur, J., 2015. Pre-treatments, characteristics, and biogeochemical dynamics of dissolved organic matter in sediments: a review. Water Res. 79, 10–25.

Chen, M., Jaffé, R., 2014. Photo- and bio-reactivity patterns of dissolved organic matter from biomass and soil leachates and surface waters in a subtropical wetland. Water Res. 61, 181–190.

Chen, Y.-J.C., Wu, S.-C., Lee, B.-S., Hung, C.-C., 2006. Behavior of storm-induced suspension interflow in subtropical feitsui reservoir, Taiwan. Limnol. Oceanogr. 51 (2), 1125–1133.

Chow, A.T., Guo, F., Gao, S., Breuer, R., Dahlgren, R.A., 2005. Filter pore size selection for characterizing dissolved organic carbon and trihalomethane precursors from soils. Water Res. 39 (7), 1255–1264.

Chow, A.T., Guo, F., Gao, S., Breuer, R., Dahlgren, R.A., 2006. Size and XAD fractionations of trihalomethane precursors from soils. Chemosphere 62 (10), 1636–1646.

Chow, A.T., Leech, D.M., Boyer, T.H., Singer, P.C., 2008. Impact of simulated solar irradiation on disinfection byproduct precursors. Environ. Sci. Technol. 42, 5586–5593.

Cuss, C.W., Guéguen, C., 2013. Distinguishing dissolved organic matter at its origin: size and optical properties of leaf-litter leachates. Chemosphere 92, 1483–1489.

Dainard, P.G., Guéguen, C., McDonald, N., Williams, W.J., 2015. Photobleaching of

fluorescent dissolved organic matter in beaufort sea and north atlantic subtropical gyre. Mar. Chem. 177, 630–637.
Derrien, M., Kim, M.-S., Ock, G., Hong, S., Cho, J., Shin, K.-H., Hur, J., 2018. Estimation of different source contributions to sediment organic matter in an agricultural-forested watershed using end member mixing analyses based on stable isotope ratios and fluorescence spectroscopy. Sci. Total Environ. 618, 569–578.
Derrien, M., Yang, L., Hur, J., 2017. Lipid biomarkers and spectroscopic indices for identifying organic matter sources in aquatic environments: a review. Water Res. 112, 58–71.
Garcia, R.D., Diéguez, M.C., Gerea, M., Garcia, P.E., Reissig, M., 2018. Characterisation and reactivity continuum of dissolved organic matter in forested headwater catchments of Andean Patagonia. Freshw. Biol. 1–14.
Goldthwait, S.A., Carlson, C.A., Henderson, G.K., Alldredge, A.L., 2005. Effects of physical fragmentation on remineralization of marine snow. Mar. Ecol. Prog. Ser. 305, 59–65.
Golea, D.M., Upton, A., Jarvis, P., Moore, G., Sutherland, S., Parsons, S.A., Judd, S.J., 2017. THM and HAA formation from NOM in raw and treated surface waters. Water Res. 112, 226–235.
Graeber, D., Gelbrecht, J., Pusch, M.T., Anlanger, C., von Schiller, D., 2012. Agriculture has changed the amount and composition of dissolved organic matter in Central European headwater streams. Sci. Total Environ. 438, 435–446.
He, W., Jung, H., Lee, J.-H., Hur, J., 2016a. Differences in spectroscopic characteristics between dissolved and particulate organic matters in sediments: insight into distribution behavior of sediment organic matter. Sci. Total Environ. 547, 1–8.
He, W., Chen, M., Schlautman, M.A., Hur, J., 2016b. Dynamic exchanges between DOM and POM pools in coastal and inland aquatic ecosystems: a review. Sci. Total Environ. 551–552, 415–428.
Helms, J.R., Stubbins, A., Ritchie, J.D., Minor, E.C., Kieber, D.J., Mopper, K., 2008. Absorption spectral slopes and slope ratios as indicators of molecular weight, source, and photobleaching of chromophoric dissolved organic matter. Limnol. Oceanogr. 53 (3), 955–969.
Hu, B., Wang, P., Zhang, N., Wang, C., Ao, Y., 2016. Photoproduction of dissolved organic carbon and inorganic nutrients from resuspended lake sediments. Environ. Sci. Pollut. Res. 23, 22126–22135.
Hua, G., Reckhow, D.A., 2007. Characterization of disinfection byproduct precursors based on hydrophobicity and molecular size. Environ. Sci. Technol. 41 (9), 3309–3315.
Huguet, A., Vacher, L., Relexans, S., Saubusse, S., Froidefond, J.M., Parlanti, E., 2009. Properties of fluorescent dissolved organic matter in the Gironde Estuary. Org. Geochem. 40, 706–719.
Hur, J., 2011. Microbial changes in selected operational descriptors of dissolved organic matters from various sources in a watershed. Water Air Soil Pollut. 215 (1–4), 465–476.
Hur, J., Park, M.-H., Schlautman, M.A., 2009. Microbial transformation of dissolved leaf litter organic matter and its effects on selected organic matter operational descriptors. Environ. Sci. Technol. 43 (7), 2315–2321.
Hur, J., Jung, K.-Y., Jung, Y.M., 2011. Characterization of spectral responses of humic substances upon UV irradiation using two-dimensional correlation spectroscopy. Water Res. 45 (9), 2965–2974.
Hur, J., Jung, N.-C., Shin, J.-K., 2007. Spectroscopic distribution of dissolved organic matter in a dam reservoir impacted by turbid storm runoff. Environ. Monit. Assess. 133 (1–3), 53–67.
Hur, J., Schlautman, M.A., 2003. Molecular weight fractionation of humic substances by adsorption to minerals. J. Colloid Interface Sci. 264, 313–321.
Kieber, R.J., Whitehead, R.F., Skrabal, S.A., 2006. Photochemical production of dissolved organic carbon from resuspended sediments. Limnol. Oceanogr. 51 (5), 2187–2195.
Kleber, M., Sollins, P., Sutton, R., 2007. A conceptual model of organo-mineral interactions in soils: self-assembly of organic molecular fragments into zonal structures on mineral surfaces. Biogeochemistry 85, 9–24.
Koelmans, A.A., Prevo, L., 2003. Production of dissolved organic carbon in aquatic sediment suspensions. Water Res. 37 (9), 2217–2222.
Lee, B.M., Seo, Y.-S., Hur, J., 2015. Investigation of adsorptive fractionation of humic acid on graphene oxide using fluorescence EEM-PARAFAC. Water Res. 73, 242–251.
Lee, K.C., Lee, W.T., 2015. Effects of pH, water temperature and chlorine dosage on the formation of disinfection byproducts at water preatment plant. J. Korean Soc. Environ. Eng. 37 (9), 505–510.
Lee, M.H., Hur, J., 2014. Photodegradation-induced changes in the characteristics of dissolved organic matter with different sources and their effects on disinfection by-product formation potential. Clean. - Soil, Air, Water 42 (5), 552–560.
Lee, M.H., Payeur-Poirier, J.L., Park, J.H., Matzner, E., 2016. Variability in runoff fluxes of dissolved and particulate carbon and nitrogen from two watersheds of different tree species during intense storm events. Biogeosciences 13, 5421–5432.
Lee, M.H., Ok, Y.S., Hur, J., 2018. Dynamic variations in dissolved organic matter and the precursors of disinfection by-products leached from biochar: leaching experiments simulating intermittent rain events. Environ. Pollut. 242, 1912–1920.
Li, W.-T., Chen, S.-Y., Xu, Z.-X., Li, Y., Shuang, C.-D., Li, A.-M., 2014. Characterization of dissolved organic matter in municipal wastewater using fluorescence PARAFAC analysis and chromatography multi-excitation/emission scan: a comparative study. Environ. Sci. Technol. 48 (5), 2603–2609.
Liu, Q., Shank, G.C., 2015. Solar radiation-enhanced dissolution (photodissolution) of particulate organic matter in Texas estuaries. Estuar. Coasts 38 (6), 2172–2184.
Maqbool, T., Hur, J., 2016. Changes in fluorescent dissolved organic matter upon interaction with anionic surfactant as revealed by EEM-PARAFAC and two-dimensional correlation spectroscopy. Chemosphere 161, 190–199.
Mayer, L.M., Schick, L.L., Bianchi, T.S., Wysocki, L.A., 2009. Photochemical changes in chemical markers of sedimentary organic matter source and age. Mar. Chem. 113 (1–2), 123–128.
Mayer, L.M., Thornton, K.R., Schick, L.L., Jastrow, J.D., Harden, J.W., 2012. Photodissolution of soil organic matter. Geoderma 170, 314–321.
McKnight, D.M., Boyer, E.W., Westerhoff, P.K., Doran, P.T., Kulbe, T., Andersen, D.T., 2001. Spectrofluorometric characterization of dissolved organic matter for indication of precursor organic material and aromaticity. Limnol. Oceanogr. 46, 38–48.
Mostofa, K.M.G., Yoshioka, T., Konohira, E., Tanoue, E., 2007. Photodegradation of fluorescent dissolved organic matter in river waters. Geochem. J. 41 (5), 323–331.
Murphy, K.R., Stedmon, C.A., Waite, T.D., Ruiz, G.M., 2008. Distinguishing between terrestrial and autochthonous organic matter sources in marine environments using fluorescence spectroscopy. Mar. Chem. 108 (1–2), 40–58.
Murphy, K.R., Stedmon, C.A., Graeber, D., Bro, R., 2013. Fluorescence spectroscopy and multi-way techniques. PARAFAC. Anal. Methods 5, 6557.
Murphy, K.R., Stedmon, C.A., Wenig, P., Bro, R., 2014. OpenFluor- an online spectral library of auto-fluorescence by organic compounds in the environment. Anal. Methods 6, 658–661.
Nimptsch, J., Woelfl, S., Osorio, S., Valenzuela, J., Ebersbach, P., von Tuempling, W., Palma, R., Encina, F., Figueroa, D., Kamjunke, N., Graeber, D., 2015. Tracing dissolved organic matter (DOM) from land-based aquaculture systems in North Patagonian streams. Sci. Total Environ. 537, 129–138.
Osburn, C.L., Handsel, L.T., Mikan, M.P., Paerl, H.W., Montgomery, M.T., 2012. Fluorescence tracking of dissolved and particulate organic matter quality in a river-dominated estuary. Environ. Sci. Technol. 46 (16), 8628–8636.
Phong, D.D., Hur, J., 2015. Insight into photocatalytic degradation of dissolved organic matter in UVA/TiO_2 systems revealed by fluorescence EEM-PARAFAC. Water Res. 87, 119–126.
Pifer, A.D., Fairey, J.L., 2012. Improving on $SUVA_{254}$ using fluorescence-PARAFAC analysis and asymmetric flow-field flow fractionation for assessing disinfection byproduct formation and control. Water Res. 46 (9), 2927–2936.
Pifer, A.D., Fairey, J.L., 2014. Suitability of organic matter surrogates to predict trihalomethane formation in drinking water sources. Environ. Eng. Sci. 31 (3), 117–126.
Ruecker, A., Uzun, H., Karanfil, T., Tsui, M.T.K., Chow, A.T., 2017. Disinfection byproduct precursor dynamics and water treatability during an extreme flooding event in a coastal blackwater river in southeastern United States. Chemosphere 188, 90–98.
Shank, G.C., Evans, A., Yamashita, Y., Jaffé, R., 2011. Solar radiation-enhanced dissolution of particulate organic matter from coastal marine sediments. Limnol. Oceanogr. 56 (2), 577–588.
Shin, J.K., Jeong, S.A., Choi, I., Hwang, S.J., 2004. Dynamics of turbid water in a Korean reservoir with selective withdrawal discharges. Korean J. Limnol. 37 (4), 423–430.
Soto Cárdenas, C., Gerea, M., Garcia, P.E., Pérez, G.L., Diéguez, M.C., Rapacioli, R., Reissig, M., Queimaliños, C., 2017. Interplay between climate and hydrogeomorphic features and their effect on the seasonal variation of dissolved organic matter in shallow temperate lakes of the Southern Andes (Patagonia, Argentina): a field study based on optical properties. Ecohydrology 10, e1872.
Southwell, M.W., Kieber, R.J., Mead, R.N., Brooks, A.G., Skrabal, S.A., 2010. Effects of sunlight on the production of dissolved organic and inorganic nutrients from resuspended sediments. Biogeochemistry 98, 115–126.
Timko, S.A., Gonsior, M., Cooper, W.J., 2015. Influence of pH on fluorescent dissolved organic matter photo-degradation. Water Res. 85, 266–274.
Water Information System, 2018. cited 25. 05. 2018; Available on Internet: http://water.nier.go.kr.
Weishaar, J.L., Aiken, G.R., Bergamaschi, B.A., Fram, M.S., Fujii, R., Mopper, K., 2003. Evaluation of specific ultraviolet absorbance as an indicaor of the chemical composition and reactivity of dissolved organic carbon. Environ. Sci. Technol. 37 (20), 4702–4708.
Worrall, F., Burt, T.P., Howden, N.J.K., Hancock, G.R., Wainwright, J., 2018. The fate of suspended sediment and particulate organic carbon in transit through the channels of a river catchment. Hydrol. Process. 32 (1), 146–159.
Yamashita, Y., Jaffé, R., 2008. Characterizing the interactions between trace metals and dissolved organic matter using excitation-emission matrix and parallel factor analysis. Environ. Sci. Technol. 42 (19), 7374–7379.
Yang, L., Kim, D., Uzun, H., Karanfil, T., Hur, J., 2015. Assessing trihalomethanes (THMs) and *N*-nitrosodimethylamine (NDMA) formation potentials in drinking water treatment plants using fluorescence spectroscopy and parallel factor analysis. Chemosphere 121, 84–91.
Yang, L., Zhyang, W.-E., Chen, C.-T.A., Wang, B.-J., Kuo, F.-W., 2017a. Unveiling the transformation and bioavailability of dissolved organic matter in contrasting hydrothermal vents using fluorescence EEM-PARAFAC. Water Res. 111, 195–203.
Yang, X., Zhou, Z., Raju, M.N., Cai, X., Meng, F., 2017b. Selective elimination of chromophoric and fluorescent dissolved organic matter in a full-scale municipal wastewater treatment plant. Science (Washington, D.C.) 57, 150–161.
Yu, H., Song, Y., Gao, H., Liu, L., Yao, L., Peng, J., 2015. Applying fluorescence spectroscopy and multivariable analysis to characterize structural composition of dissolved organic matter and its correlation with water quality in an urban river. Environmental Earth Sciences 73, 5163–5171.

Zhang, Y., Liu, M., Qin, B., Feng, S., 2009. Photochemical degradation of chromophoric-dissolved organic matter exposed to simulated UV-B and natural solar radiation. Hydrobiologia 627, 159–168.
Zimmermann-Timm, H., 2002. Characteristics, dynamics and importance of aggregates in rivers-an invited review. Int. Rev. Hydrobiol. 87 (2–3), 197–240.
Zsolnay, A., Baigar, E., Jimenez, M., Steinweg, B., Saccomandi, F., 1999. Differentiating with fluorescence spectroscopy the sources of dissolved organic matter in soils subjected to drying. Chemosphere 38, 45–50.